Ultra-high-Q phononic resonators on-chip at cryogenic temperatures

Ultra-high-Q phononic resonators on-chip at cryogenic temperatures

Prashanta Kharel, Yiwen Chu, Michael Power, William H. Renninger, Robert J. Schoelkopf, and Peter T. Rakich

Citation: APL Photonics **3**, 066101 (2018); doi: 10.1063/1.5026798
View online: https://doi.org/10.1063/1.5026798
View Table of Contents: http://aip.scitation.org/toc/app/3/6
Published by the American Institute of Physics

Ultra-high-*Q* phononic resonators on-chip at cryogenic temperatures

Prashanta Kharel,[a] Yiwen Chu, Michael Power, William H. Renninger, Robert J. Schoelkopf, and Peter T. Rakich[b]
Department of Applied Physics, Yale University, New Haven, Connecticut 06511, USA

(Received 23 February 2018; accepted 23 April 2018; published online 21 May 2018)

Long-lived, high-frequency phonons are valuable for applications ranging from optomechanics to emerging quantum systems. For scientific as well as technological impact, we seek high-performance oscillators that offer a path toward chip-scale integration. Confocal bulk acoustic wave resonators have demonstrated an immense potential to support long-lived phonon modes in crystalline media at cryogenic temperatures. So far, these devices have been macroscopic with cm-scale dimensions. However, as we push these oscillators to high frequencies, we have an opportunity to radically reduce the footprint as a basis for classical and emerging quantum technologies. In this paper, we present novel design principles and simple microfabrication techniques to create high performance chip-scale confocal bulk acoustic wave resonators in a wide array of crystalline materials. We tailor the acoustic modes of such resonators to efficiently couple to light, permitting us to perform a non-invasive laser-based phonon spectroscopy. Using this technique, we demonstrate an acoustic Q-factor of 2.8×10^7 (6.5×10^6) for chip-scale resonators operating at 12.7 GHz (37.8 GHz) in crystalline z-cut quartz (x-cut silicon) at cryogenic temperatures.
https://doi.org/10.1063/1.5026798

I. INTRODUCTION

Acoustic-wave technologies have become indispensable for everything from classical signal processing[1] to precision metrology.[2] Rapid advancements in quantum optics, optomechanics, and circuit quantum electrodynamics have recently spurred interest in phonons as the basis for emerging quantum technologies.[3–7] In these systems, phonons become coherent carriers of information and can also be utilized to mediate interactions between different types of excitations (such as optical photons, microwaves, and defect centers).[5,7–11] In this context, we seek high quality-factor (Q) phonon modes at high frequencies (f), making the $f \cdot Q$-product a key figure of merit.[4,8] Such high frequency (GHz) phonons are easily cooled to their quantum ground states and can be used to store quantum states for extended periods of time. Low temperature operation has the added benefit that phonon lifetimes are radically enhanced in pristine crystalline media. As a basis for emerging quantum technologies,[7] we seek high performance phononic resonators that offer a path toward chip-scale integration.

While there are many promising approaches to size reduction for mechanical resonators,[12] the task of achieving high $f \cdot Q$ products within a small package at cryogenic temperatures introduces a unique set of challenges. To dramatically extend phonon lifetimes, we seek to eliminate extrinsic sources of loss.[13,14] In this regard, phononic crystal-based device strategies offer an intriguing solution,[15–18] as they can theoretically eliminate external loss channels through the formation of complete phononic bandgaps. Bulk acoustic wave (BAW) resonators offer a complementary path to high performance at cryogenic temperatures. For instance, record $f \cdot Q$ products (1.6×10^{18}) have

[a]prashanta.kharel@yale.edu
[b]peter.rakich@yale.edu

been demonstrated at microwave (200 MHz) frequencies using confocal BAW resonators that mitigate extrinsic losses by trapping the phonon modes within the bulk of a pristine crystal.[19] However, because these devices are typically designed for operation at relatively low frequencies (5-100 MHz), they have historically been relatively large (centimeter-scale).[20] Fortunately, as we scale to higher phonon frequencies, smaller acoustic wavelength permits radical reductions in size. These resonators are comparatively simple to fabricate and have great versatility; individual resonators support high-Q phonon modes over a wide range of frequencies (1-100 GHz) and can be formed from an array of different materials.

In this paper, we present novel design principles and simple fabrication techniques to create high performance BAW resonators on-chip. Through these studies, we use non-invasive optical techniques to quantify the performance of acoustic resonators that are created from both quartz and silicon substrates. To access the acoustic modes using light, we engineer the elastic modes of the resonators to produce efficient light-sound coupling through intrinsic photoelastic response. This general strategy, which can be used to study phonon modes within practically any transparent material, permits us to perform non-invasive laser-based phonon spectroscopy at high frequencies (10-40 GHz). Using these device strategies and measurement approach, we demonstrate Q-factors of 2.8×10^7 (6.5×10^6) for 12.7 GHz (37.8 GHz) phonon modes of microfabricated resonators in z-cut quartz (x-cut silicon) at 10.3 K (8.0 K). Remarkably, these chip-scale BAW resonators exhibit $f \cdot Q$ products on par with previously demonstrated values in macroscopic (cm-scale) BAW resonators[21] but in a much smaller package, with >1000-fold reduction in device volumes. The design guidelines and robust fabrication techniques presented here can be generalized to create chip-scale BAW resonators on a wide array of materials.

II. DEVICE DESIGN

The device under study consists of a microfabricated plano-convex BAW resonator on-chip [see Fig. 1(a)], which we call confocal High-Overtone Bulk Acoustic Resonator (cHBAR). Microfabrication permits the creation of compact devices with diameters ranging from tens of microns up to a few millimeters. Longitudinal acoustic phonons are trapped within this system as the acoustic wave

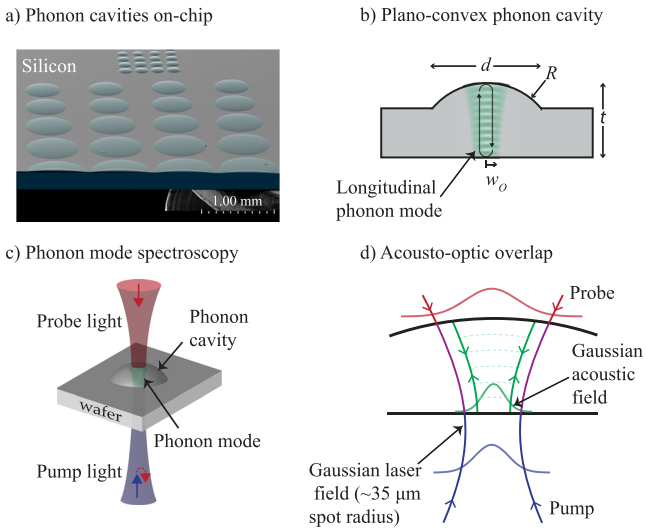

FIG. 1. (a) False-color scanning electron microscope image of arrays of plano-convex bulk acoustic wave resonators microfabricated on a silicon chip. Phonon cavity geometry can be easily tailored for resonators fabricated on-chip. (b) These resonators have plano-convex geometry that permits tight confinement of standing-wave longitudinal phonon modes near the center of the device (acoustic waist radius $w_o < 40$ μm). (c) These longitudinal acoustic modes couple to counter-propagating optical fields through photoelastic coupling, which is used to perform non-invasive laser-based spectroscopy of phonon modes at GHz frequencies. (d) For sensitive optomechanical spectroscopy, we seek to maximize the acousto-optic overlap with Gaussian laser fields with spot sizes of ~35 μm.

reflects from both top and bottom surfaces of the substrate resulting in standing-wave phonon modes [see Fig. 1(b)]. This plano-convex design mitigates acoustic diffraction and produces confinement of acoustic energy in the transverse dimension (typical acoustic beam radius is <40 μm). Since these acoustic modes live primarily in the bulk medium, they have greatly reduced surface interactions, making them less susceptible to scattering losses.

Phonon mode spectroscopy is performed using a non-invasive laser-based approach described in Ref. 21; stimulated energy transfer between counter-propagating light fields occurs as the detuning between the two light fields is swept near the Brillouin frequency [see Fig. 1(c)]. This energy transfer spectrum gives us information about the frequencies and lifetimes of the phonons. To permit efficient optical access to the resonator modes, we also tailor the plano-convex geometry to enhance optomechanical coupling with the incident Gaussian laser fields of spot sizes of ∼35 μm [see Fig. 1(d)]. Before we explore this optomechanical coupling in greater detail, we explain the design principles and fabrication methods used to create chip-scale cHBAR.

We are greatly able to reduce the size of the resonators by exploiting the fact that acoustic wavelengths are greatly reduced at high frequencies. Since the wavelengths ($\lambda_{ph} < 1$ μm) of these high frequency phonons are much smaller than the system dimensions (hundreds of microns), the acoustic wave propagation becomes reminiscent of optical beam propagation in the paraxial limit. We show that these plano-convex phonon resonators support high Q-factor mode families, with Hermite-Gaussian-like mode profiles (see the supplementary material for details); these acoustic modes are engineered to have good acousto-optic overlap with the Gaussian laser fields. Next, we adopt established methods from optics to design stable, high-Q cHBAR.

Within the framework of Gaussian beam optics, we expect only certain radii of curvatures to form stable cavities; in a stable optical cavity, transverse spatial confinement occurs because the reflections from the resonator surfaces compensate for effects of diffraction.[22] Stability criteria for a Fabry-Pérot optical cavity in vacuum consisting of two mirrors with radii of curvatures R_1 and R_2 separated by a distance of L are given by $0 \leq g_1 g_2 \leq 1$, where the stability parameter is defined as $g_i = 1 - L/R_i (i = 1, 2)$.[23] In the context of acoustics, correctly formulated stability parameters g_1 and g_2 must account for the anisotropy of elastic constants. In contrast to optical waves propagating in vacuum, acoustic beam propagation in anisotropic crystalline media can be non-trivial; the sound velocities for different polarization components can change dramatically depending on the propagation direction. The slowness surface, which is analogous to ray surface in optics, characterizes acoustic beam propagation as the group velocity is normal to this surface.[24] While ray surfaces for optical beams propagating in vacuum are symmetric and parabolic, the acoustic slowness surfaces can be asymmetric and non-parabolic about the propagation axis.[25] However, we can greatly simplify the acoustic resonator design by choosing crystalline axes about which the slowness surfaces are parabolic and symmetric. In this case, we can formulate stability criteria that closely mirror laser beam optics in the paraxial limit (see the supplementary material for details). The stability parameters for plano-convex phononic cavities formed using z-cut quartz and x-cut silicon are simply given by

$$g_1 = 1, \; g_2 = 1 - \frac{t}{\chi R}, \tag{1}$$

where t is the thickness of the wafer, R is the radius of curvature of the convex surface, and χ is an "anisotropy-constant" that includes the effect of propagation of acoustic beam in an anisotropic medium. For acoustic beam propagation perpendicular to the z-cut face of quartz and x-cut face of silicon, χ can be calculated analytically yielding $\chi_{Si} = 0.6545$ and $\chi_{Quartz} = 0.5202$ (see the supplementary material for details). Therefore, the range of the radius of curvatures that can produce stable plano-convex phonon cavities is $0 \leq 1 - t/(\chi R) \leq 1$ or equivalently $R \geq t/\chi$. For the design of phonon cavities along crystalline axes in the case when the symmetry requirement is not satisfied (i.e., non-trivial dispersion surfaces with asymmetric or non-parabolic dispersion surfaces), more sophisticated methods such as the numerical acoustic beam propagation techniques discussed in Ref. 21 must be used.

In addition to forming a stable phonon cavity, we choose the radius of curvature R to enhance the acousto-optic coupling. Since the acousto-optic coupling depends on the overlap integral between the optical and acoustic modes,[21] we seek to maximize coupling for the fundamental acoustic mode

by matching the acoustic beam waist to the optical beam waist. The acoustic waist radius, w_o, at the planar surface can be expressed in terms of R as

$$w_o^2 = \frac{t\lambda_{\mathrm{ph}}}{\chi\pi}\sqrt{\frac{g_1g_2(1-g_1g_2)}{(g_1+g_2-2g_1g_2)^2}}, \tag{2}$$

where λ_{ph} is the wavelength of the phonon mode. For instance, a 1-mm-thick plano-convex phonon cavity in z-cut quartz with $R = 65$ mm supports a 12.66 GHz acoustic mode having $w_o = 39.6$ μm. Therefore, by changing R, we can tailor the acoustic mode so that it couples efficiently to a focused laser beam of radius ∼35 μm used in our experiments. Finally, we chose the diameter of the phonon cavity, d, to be much larger than the phonon beam waist, w_o [see Fig. 1(b)]. This ensures that the exponential tails of the acoustic Gaussian beam are vanishingly small where the convex surface terminates, meaning the diffractive (or anchoring losses) are negligible. For instance, assuming all the energy outside the convex surface is lost to diffractive losses, for $d/w_o = 5$, we still find that the Q-factor limit due to this loss mechanism would be 7×10^9 (1.5×10^{10}) for the phonon cavities fabricated on quartz (silicon) (see the supplementary material for details). For a phonon cavity with a given thickness and radius of curvature, Eq. (2) reveals that phonons at higher frequencies have a smaller waist radius (i.e., $w_o \propto 1/\sqrt{f}$). Therefore, as we seek operation at high frequencies, the phonon mode volume shrinks, permitting us to fabricate smaller phononic devices.

III. FABRICATION

Next, we give an overview of the fabrication steps used to fabricate these phonon cavities. We developed simple microfabrication techniques to create high performance phononic oscillators on-chip by leveraging strategies used to fabricate optical micro-lenses.[26–28] However, to achieve low loss phonon modes at high frequencies (having $\lambda_{\mathrm{ph}} \lessapprox 500$ nm), we optimized the fabrication process to yield resonators having excellent surface finish. Standard optical lithography allowed us to print cylindrical photoresist patterns which are transformed into hemispheres using a solvent vapor reflow technique [see Fig. 2(a)]. Photoresist structures became less viscous after absorbing solvent vapor, allowing surface tension to form photoresist hemispheres having excellent surface roughness (∼1 nm). This reflow also permits us to form photoresist hemispheres having large radii of curvature (tens of mm). Additionally, the center height of the photoresist hemispheres after solvent vapor reflow is not dependent on the substrate material and is relatively insensitive to the photoresist diameters.[29] In this way, we can change the radius of curvature by independently changing the thickness or the diameter of the photoresist cylinders.

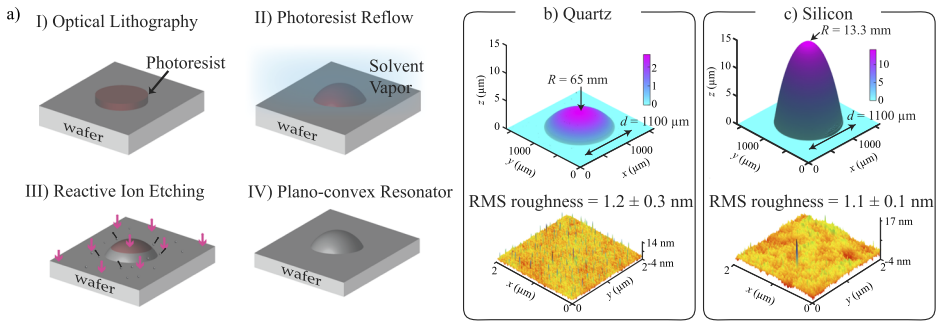

FIG. 2. (a) Microfabrication steps taken to fabricate plano-convex phononic resonators on-chip. (I) Standard optical lithography is used to write cylindrical photoresist patterns. (II) This photoresist cylinder is reflowed into a hemisphere using the solvent-vapor reflow technique. (III) Reactive ion etching (RIE) is used to transfer the hemispherical pattern onto the substrate. (IV) After completely etching away the photoresist, we get a plano-convex cavity that supports long-lived phonon modes. Measured 3D-surface profiles of the phonon cavities in (b) z-cut quartz and (c) x-cut silicon after RIE show excellent surface quality. The difference in height (and hence the radius of curvature) is a result of difference in etch selectivity of the substrate over photoresist (ratio of the etch rate of substrate to the etch rate of photoresist). Using atomic force microscopy (AFM), we measure ∼1 nm root mean square surface roughness for phononic cavities on both quartz and silicon.

After the reflow process, hemispherical photoresist patterns are imprinted on the substrate material by completely etching away the photoresist using reactive ion etching (RIE). The ratio of the etching rate of photoresist to the etching rate of substrate material (also known as etch selectivity) determined the final radius of curvature of the phonon cavities. Reactive ion etch parameters were optimized to ensure excellent surface roughness after the etch.

In what follows, we describe fabrication steps used to make plano-convex phonon cavities in crystalline quartz and silicon on-chip. The fabrication process begins by creating photoresist hemispheres. We start with a double-sided polished 1-mm-thick z-cut quartz wafer (>A grade, 99.997% pure). To eliminate organic contaminants and adsorbates from the wafer surface, the wafer is oxygen plasma cleaned for 3 min at an RF-power of 300 W and a pressure of 300 mTorr. We then spin coated a 5.5-μm-thick layer of photoresist (AZP 4620) on the wafer and post-baked at 110 °C for 2 min to harden the photoresist. A lithographic photomask was used to define circular structures during UV exposure as seen in Fig. 2(a) (400 mJ/cm^2 at 405 nm wavelength). The exposed photoresist is developed using the 1:4 AZ400K:water developer solution. The photoresist cylinders are then vapor primed with the resist adhesion promoter hexamethyldisilizane (HMDS) for 15 min to preserve the circular geometry during reflow. The solvent vapor reflow of these photoresist cylinders is accomplished using polypropylene glycol monomethyl ether acetate (PGMEA) solvent. The solvent is heated in a closed chamber at 55 °C with the wafer placed upside down (not touching the liquid) at 60 °C until the photoresist has completely reflowed into hemispheres. After the reflow, the wafer is first baked at 90 °C for 1 min to harden the photoresist and the temperature is gradually increased to 125 °C over the course of 15 min to eliminate any solvent that remains dissolved. The center height of the photoresist hemispheres after the reflow process is approximately 10.5 μm. For this resist thickness, by simply changing the diameter of the photoresist hemispheres from 50 μm to 1.5 mm, we can vary the radii of curvature of these photoresist hemispheres from approximately hundreds of microns to 30 mm.

A slow reactive ion etch using SF_6 and Ar gases with 4 SCCM and 14 SCCM flow rates, respectively, at a low chamber pressure of 4 mTorr and a bias voltage of 370 V is used to etch away the photoresist completely. In the process, a slow erosion (a combination of chemical and physical etch at ∼35 nm/min) of the substrate occurs as shown in Fig. 2(a)–III. This results in phonon cavities with excellent surface quality. The etch selectivity of photoresist over quartz of 3.8 results in hemispheres in quartz with center height of approximately 2.7 μm. Because of the etch-selectivity, we can fabricate phonon cavities with radii of curvature as large as 110 mm in quartz by simply changing the diameter of the photoresist. However, even larger radii of curvature can be made by using thinner photoresist. Finally, the wafer is cleaned in piranha solution (3:1 sulphric acid:hydrogen peroxide) for 2 min to get rid of any organic contaminants before optical measurements.

The fabrication steps of phonon cavities on silicon are similar to those outlined for quartz earlier; only the reactive ion etching process parameters differ. We create photoresist hemispheres on a 500-μm-thick double-side-polished float-zone grown x-cut silicon wafer (resistivity >1000 Ω · cm) using the same optical lithography and solvent vapor reflow outlined for quartz. The photoresist hemispheres are then reactive ion etched using SF_6 and O_2 gases with 5 SCCM and 2 SCCM flow rates, respectively, at a chamber pressure of 10 mTorr and a bias voltage of 394 V. A slow erosion (∼100 nm/min) of the substrate gives excellent surface quality. The etch selectivity of 0.74 produces convex surfaces in silicon with center height of approximately 14.2 μm. Surface passivation of silicon using piranha etch and diluted hydrofluoric acid dip following the procedure outlined in Ref. 30 is performed before optical measurements.

The results of these fabrication processes are characterized using a 3D surface profilometer (Zygo Nexview) as seen in Figs. 2(b) and 2(c). A hemispherical surface fits well to these plano-convex phonon cavities with diameters of 1100 μm. This fitting allows us to determine the radius of curvature of 65 ± 1 mm (13.3 ± 0.3 mm) for resonators in quartz (silicon). This difference in the radius of curvatures for the same diameter cavities in two different substrates is a result of etch selectivity differences during the RIE process. We chose 65 mm radius of curvature phonon cavities in quartz for our optical measurements because, as discussed before, this results in enhanced acousto-optic overlap with the Gaussian laser fields. We chose 13.3 mm radius of curvature phonon cavities in silicon because, given a low etch selectivity of 0.74, this was the largest radius of curvature we could

obtain without significant deviation from a hemispherical surface. We observed that the photoresist hemispheres with smaller diameters ($\lesssim$1.1 mm) tend to have more axially symmetric surfaces during reflow due to the negligible effect of gravity during the reflow process.[31] The surface roughness is measured using an atomic-force microscope (Bruker Dimension Fastscan AFM). We measure a root mean square roughness of 1.2 ± 0.3 nm (1.1 ± 0.1 nm) for the etched surface in quartz (silicon). The surface quality and parabolic shape obtained through this fabrication process suggest that these on-chip resonators could potentially support high-Q bulk acoustic phonons.

IV. EXPERIMENTAL STUDIES

To quantify the performance of these phononic resonators at cryogenic temperatures, we perform a laser-based optomechanical spectroscopy. We engineer the phonon modes of our resonators to be Brillouin-active such that optical forces generated by photoelastic response of the material permits light-sound coupling. Through a phase-matched Brillouin-like interaction, laser fields can couple to high-frequency longitudinal acoustic phonon modes over a finite frequency range centered about the Brillouin frequency, $\Omega_s = 2\omega_p v_a/v_o$. Here, $v_a(v_o)$ is the speed of sound (light) in the bulk medium and ω_p is the frequency of the pump light. The bandwidth of coupling is determined by the sinc-squared response due to phase-matching constraints and is approximately equal to twice the acoustic free spectral range (FSR) of $v_a/2t$ as seen in Figs. 3(a) and 3(b). Through this interaction, the stimulated energy transfer between the counter-propagating pump and probe waves coincides with the generation of coherent phonons within the crystal [see Fig. 1(c)]. By sweeping the frequency detuning between these laser fields, we can perform high-frequency phonon spectroscopy; multiple resonances corresponding to the standing wave longitudinal phonon modes centered around Ω_s appear in the energy transfer spectrum and the linewidth of these resonances is determined by the phonon dissipation rate $\Gamma/2\pi$. This versatile technique permits us to perform phonon spectroscopy in practically any transparent crystalline medium (with or without piezoelectric response). Moreover, since this technique is non-invasive, it permits us to perform rapid spectroscopy on arrays of chip-scale phonon cavities.

In our experiment, we use the counter-propagating pump light and probe light derived from the same laser source (Pure-Photonics PCL200) at 1549 nm to obtain energy transfer spectra at cryogenic temperatures. The frequency of the pump light is fixed at the laser frequency while the detuning between the pump light and the probe light ($\Omega = \omega_p - \omega_s$) is swept through the Brillouin frequency (Ω_s). The increase in the probe power (ΔP_s) produced by the Brillouin gain as the probe wave traverses the sample is recorded as a function of Ω (details on the optomechanical coupling and measurement setup can be found in Ref. 21).

Using this form of optomechanical spectroscopy, we identify families of narrow resonances corresponding to longitudinal standing wave acoustic modes near the Brillouin frequency of 12.66 GHz (37.76 GHz) for resonators in quartz (silicon) at 10.3 K (8.0 K) [see Figs. 3(a) and 3(b)]. These mode families (m, $m + 1$, and so on) are separated by the acoustic FSR of 3.13 MHz (8.27 MHz) as expected for 1-mm-thick z-cut quartz (500-μm-thick x-cut silicon). As we examine the resonances within a single mode family (i.e., between m and $m + 1$), we observe multiple equally spaced resonances separated by 154 kHz (761 kHz) for resonators in quartz (silicon). These resonances (L1, L2, and so on) are higher order transverse phonon modes (Hermitte-Gaussian-like modes) of the plano-convex geometry. The frequency spacing for the higher order modes agrees well with the analytically calculated spacing of 155 kHz (731 kHz) (see the supplementary material for details).

For completeness, we compared our experimental results as well as the analytical theory, which approximates the dispersion surface as a paraboloid, with the numerical beam propagation method of Ref. 21, which accounts for the full anisotropy in the elastic tensor. This numerical method was used to calculate the mode spacing [blue dots in Figs. 3(c) and 3(d)] as well as the acoustic mode profiles seen in Figs. 3(c)–3(f). Note that we compare the relative mode spacing, as uncertainties in the elastic constants at cryogenic temperatures prevent us from determining the absolute mode indices (i.e., the precise number of overtones). Numerical calculations revealed good agreement with the experimental mode spacing for resonators fabricated from both quartz and silicon [see Figs. 3(c) and 3(d)]. Notice that in experiments we observe frequency splittings (~40 kHz) of higher order modes

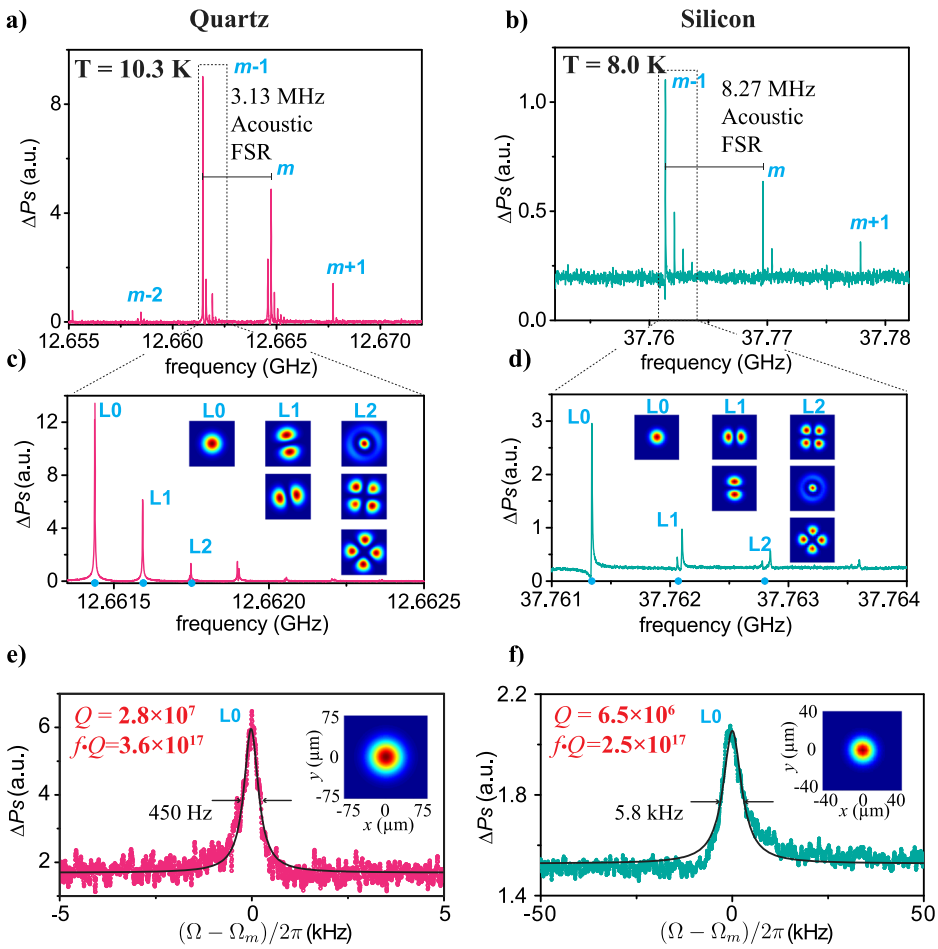

FIG. 3. Laser-based spectroscopy of standing-wave longitudinal acoustic modes in resonators in z-cut quartz (x-cut silicon) at 10.3 K (8.0 K). Back-scattered probe power (ΔP_s) was recorded as a function of frequency detuning between the pump light and the probe light. [(a) and (b)] Resonances corresponding to several longitudinal phonon modes with the mode number (m) separated by the acoustic free spectral range (FSR) of 3.13 MHz (8.27 MHz) are observed within the Brillouin-phase matching bandwidth. [(c) and (d)] As we zoom in on one acoustic FSR, we find several equally spaced resonances corresponding to higher-order transverse phonon modes (L0, L1, L2, and so on) of the plano-convex geometry. These modes have frequency spacings of 154 kHz (732 kHz) for quartz (silicon) resonators. The simulated frequency spacing (blue dots) accounting for the crystal anisotropy matches very well with the experimental results for resonators in both quartz and silicon. Simulated phonon mode intensity at the plane surface is plotted showing Hermite-Gaussian-like transverse mode profiles. [(e) and (f)] Measurement of the fundamental longitudinal mode (L0) at low optical powers reveals a narrow full-width at half-maximum (FWHM) of 450 Hz (5.8 kHz) for a phonon mode at 12.66 GHz (37.76 GHz) in quartz (silicon).

(L1 and L2) in silicon [see Fig. 3(d)]; analogous resonance splittings are obtained in the numerical simulation by taking into account the actual shape of the microfabricated surface, which has a small axial asymmetry. Notice also that at high optical powers we observe Fano line-shapes for resonances in silicon [see Figs. 3(b) and 3(d)]. These Fano line-shapes are consistent with the phenomena of free carrier-induced absorption and refractive index change;[32] such effects can be mitigated at low optical powers [see Fig. 3(d)].

In general, the most tightly confined fundamental mode (L0) within a given mode family (m) is expected to exhibit the lowest diffraction (and anchoring) losses. To explore the performance of this on-chip phononic resonator, we now focus on the fundamental phonon mode (L0). To ensure that we converge on the intrinsic phonon linewidth (i.e., eliminating possible line-shape distortions arising from optical and acoustic non-linearities), we reduce the laser powers as we perform the high resolution measurements seen in Figs. 3(e) and 3(f). At such powers, we estimate phonon intensities of ~10 Wm^{-2} (220 Wm^{-2}) in quartz (silicon). The analysis of the line-shapes in Figs. 3(e) and 3(f)

revealed a linewidth (full-width at half-maximum) of 450 Hz (5.8 kHz) corresponding to an ultra-high-Q of 2.8×10^7 (6.6×10^6) for the 12.7 GHz (37.8 GHz) phonon mode in resonators on-chip in z-cut quartz (x-cut silicon). This large $f \cdot Q$-product of 3.6×10^{17} (2.5×10^{17}) obtained for the on-chip resonator in quartz (silicon) is comparable to $f \cdot Q$-products obtained in macroscopic bulk-crystalline resonators.[19,21]

V. DISCUSSIONS

These techniques to fabricate and characterize on-chip phononic resonators could be extended to perform scalable studies of phonon dissipation, surface interactions, and defects/impurities in a broad class of materials. As for technological applications, on-chip plano-convex phononic resonators of the same form factor discussed here can be coupled to superconducting qubits.[7] While we have designed our phononic devices to have high Q at >10 GHz corresponding to the Brillouin frequency, these design strategies can be used to create chip-scale cHBAR that supports low-loss phonon modes in frequency ranges (5-10 GHz) relevant to these superconducting circuits. Since the lifetimes of these phonon modes can be much longer than the superconducting qubit lifetimes, such resonators could enable the storage of quantum information on-chip.[7]

In conclusion, these results lay a foundation for versatile non-invasive material spectroscopy techniques and new device strategies to benefit quantum information. We have developed simple microfabrication techniques to fabricate arrays of phononic resonators on-chip and precisely control their geometry. Through laser-based spectroscopy of 12.7 GHz phonon modes of cHBAR in quartz at cryogenic temperatures (10.3 K), we have demonstrated $f \cdot Q$-products (3.6×10^{17}) that are comparable to the world class $f \cdot Q$-products obtained on centimeter-scale BAW quartz resonators.[21] Furthermore, our demonstration of a comparable $f \cdot Q$-product (2.5×10^{17}) in silicon at record-high frequency of 37.8 GHz at cryogenic temperatures (8 K) suggests silicon as a great platform to support long-lived high-frequency mechanical excitations. Finally, there is a path to efficiently access these high-Q phonons with both light and microwave using optomechanical and electromechanical techniques. Therefore, these chip-scale cHBAR systems could potentially enable coherent information transfer from the microwave to optical domain. Finally, it is intriguing to consider the possibility of utilizing these resonators in silicon to realize novel solid-state quantum devices consisting of spin qubits coherently coupled to both photons and phonons.[11,33]

SUPPLEMENTARY MATERIAL

See supplementary material for the complete description of stability criteria for cHBAR, anisotropy parameter, and anchoring loss estimates.

ACKNOWLEDGMENTS

We acknowledge funding support from ONR YIP (No. N00014-17-1-2514), NSF MRSEC (No. DMR-1119826), the Packard Fellowship for Science and Engineering, and the U.S. Army Research Office (No. W911NF-14-1-0011). Facilities' use was supported by the Yale SEAS cleanroom, the Yale West Campus cleanroom, and the Yale Institute for Nanoscience and Quantum Engineering (YINQE). The authors thank Luigi Frunzio, Eric Kittlaus, Nils Otterstrom, and Shai Gertler for helpful discussions and feedback. We greatly appreciate the support of our cleanroom staff: Chris Tillinghast, James Agresta, and Min Li. The authors of this paper are contributors to patent application No. 62/465101 related to Bulk Crystalline Optomechanics and patent application No. 62/465101 related to Techniques for Coupling Qubits to Acoustic Resonators and Related Systems and Methods, which were submitted by Yale University.

[1] L. Lin, R. T. Howe, and A. P. Pisano, J. Microelectromech. Syst. **7**, 286 (1998).
[2] A. Miklós, P. Hess, and Z. Bozóki, Rev. Sci. Instrum. **72**, 1937 (2001).
[3] M. Blencowe, Phys. Rep. **395**, 159 (2004).
[4] M. Aspelmeyer, T. J. Kippenberg, and F. Marquardt, Rev. Mod. Phys. **86**, 1391 (2014).
[5] A. D. O'Connell, M. Hofheinz, M. Ansmann, R. C. Bialczak, M. Lenander, E. Lucero, M. Neeley, D. Sank, H. Wang, M. Weides *et al.*, Nature **464**, 697 (2010).

[6] M. V. Gustafsson, T. Aref, A. F. Kockum, M. K. Ekström, G. Johansson, and P. Delsing, Science **346**, 207 (2014).
[7] Y. Chu, P. Kharel, W. H. Renninger, L. D. Burkhart, L. Frunzio, P. T. Rakich, and R. J. Schoelkopf, Science **358**, 199 (2017).
[8] M. Poot and H. S. van der Zant, Phys. Rep. **511**, 273 (2012).
[9] T. Palomaki, J. Harlow, J. Teufel, R. Simmonds, and K. Lehnert, Nature **495**, 210 (2013).
[10] R. Andrews, A. Reed, K. Cicak, J. Teufel, and K. Lehnert, Nature Commun. **6**, 10021 (2015).
[11] Ö. Soykal, R. Ruskov, and C. Tahan, Phys. Rev. Lett. **107**, 235502 (2011).
[12] R. Aigner, Sens. Update **12**, 175 (2003).
[13] J. Gomis-Bresco, D. Navarro-Urrios, M. Oudich, S. El-Jallal, A. Griol, D. Puerto, E. Chavez, Y. Pennec, B. Djafari-Rouhani, F. Alzina *et al.*, Nat. Commun. **5**, 4452 (2014).
[14] D. T. Nguyen, W. Hease, C. Baker, E. Gil-Santos, P. Senellart, A. Lemaître, S. Ducci, G. Leo, and I. Favero, New J. Phys. **17**, 023016 (2015).
[15] R. H. Olsson III and I. El-Kady, Meas. Sci. Technol. **20**, 012002 (2008).
[16] M. Eichenfield, J. Chan, R. M. Camacho, K. J. Vahala, and O. Painter, Nature **462**, 78 (2009).
[17] A. H. Safavi-Naeini, J. T. Hill, S. Meenehan, J. Chan, S. Gröblacher, and O. Painter, Phys. Rev. Lett. **112**, 153603 (2014).
[18] S. Hong, R. Riedinger, I. Marinkovic, A. Wallucks, S. G. Hofer, R. A. Norte, M. Aspelmeyer, and S. Gröblacher, Science **358**(6360), 203 (2017).
[19] S. Galliou, M. Goryachev, R. Bourquin, P. Abbé, J. P. Aubry, and M. E. Tobar, Sci. Rep. **3**, 2132 (2013).
[20] R. Besson, in *31st Annual Symposium on Frequency Control* (IEEE, 1977), pp. 147–152.
[21] W. Renninger, P. Kharel, R. Behunin, and P. Rakich, "Bulk crystalline optomechanics," Nat. Phys. (published online).
[22] B. E. Saleh, M. C. Teich, and B. E. Saleh, *Fundamentals of Photonics* (Wiley, New York 1991), Vol. 22.
[23] A. E. Siegman, *Lasers* (Mill Valley, CA, 1986), Vol. 37, p. 462.
[24] B. A. Auld, *Acoustic Fields and Waves in Solids* (Рипол Классик, 1973).
[25] D. Royer and E. Dieulesaint, *Elastic Waves in Solids I: Free and Guided Propagation* (Springer-Verlag, New York, 2000), pp. 177–215.
[26] Z. D. Popovic, R. A. Sprague, and G. N. Connell, Appl. Opt. **27**, 1281 (1988).
[27] M. Eisner and J. Schwider, Opt. Eng. **35**, 2979 (1996).
[28] L. Li, T. Abe, and M. Esashi, Sens. Actuators, A **114**, 496 (2004).
[29] A. Emadi, H. Wu, S. Grabarnik, G. De Graaf, and R. Wolffenbuttel, J. Micromech. Microeng. **19**, 074014 (2009).
[30] M. Borselli, T. J. Johnson, and O. Painter, Appl. Phys. Lett. **88**, 131114 (2006).
[31] H. Ren, S. Xu, and S.-T. Wu, Opt. Commun. **283**, 3255 (2010).
[32] H. Shin, W. Qiu, R. Jarecki, J. A. Cox, R. H. Olsson III, A. Starbuck, Z. Wang, and P. T. Rakich, Nat. Commun. **4**, 1944 (2013).
[33] R. Ruskov and C. Tahan, J. Phys.: Conf. Ser. **398**, 012011 (2012).